Journal of Solid State Chemistry 184 (2011) 59–63

Contents lists available at ScienceDirect

Journal of Solid State Chemistry

journal homepage: www.elsevier.com/locate/jssc

Tunable photoluminescence of $NaYF_4$:Eu nanocrystals by Sr^{2+} codoping

Guofeng Wang [a,b], Qing Peng [a,*]

[a] Department of Chemistry and State Key Laboratory of New Ceramics and Fine Processing, Tsinghua University, Beijing 100084, PR China
[b] Key Laboratory of Functional Inorganic Material Chemistry, Ministry of Education of the People's Republic of China, Heilongjiang University, Harbin 150080, PR China

ARTICLE INFO

Article history:
Received 7 July 2010
Received in revised form
8 October 2010
Accepted 25 October 2010
Available online 30 October 2010

Keywords:
Nanocrystals
$NaYF_4$
Rare earth
Tunable luminescence

ABSTRACT

$NaYF_4$:Eu/Sr nanocrystals were synthesized by a hydrothermal method. Tunable photoluminescence of the $NaYF_4$:Eu nanocrystals was successfully achieved by codoping with Sr^{2+} ions. With increasing Sr^{2+} concentration, not only the X-ray diffraction peaks of the nanocrystals become broader, but also the positions of them shift toward larger lattice parameters. Eu^{3+} and Eu^{2+} have been found to coexist in an $NaYF_4$:Eu/Sr. The Eu^{3+}/Eu^{2+} emission intensity ratio changed with the Sr^{2+} concentration and excitation wavelength. More interestingly, the spectral configurations of Eu^{2+} and Eu^{3+} also varied with the excitation wavelength, indicating that the nanocrystals have multiple luminescence centers or emitting states.

1. Introduction

In recent years, a great deal of research effort has been devoted to the synthesis of nanocrystals doped with rare earth (RE) ions driven by the fact that doped nanocrystalline phosphors have potential applications in lasers, optical telecommunication, optoelectronic devices, diagnostics, and biological labels [1–14]. Nanosized phosphors or optoelectronic devices usually exhibit novel capabilities, such as tunable wavelengths, high efficiencies, and rapid responsibilities [15–17], resulting from the quantum effects and a high surface-to-volume ratio compared to their bulk counterparts.

It is well known that fluorides, such as $NaYF_4$, LaF_3, YF_3, and CaF_2, are efficient hosts for luminescent centers, due to their low phonon energies and optical transparency over a wide wavelength range [18–25]. Recently, Chen et al. have reported that $NaGdF_4$ is also an attractive host for phosphors with interesting upconversion luminescent properties [26]. Even so, $NaYF_4$ is still acknowledged as one of the most efficient host lattices for *RE* ions.

The luminescence properties of *RE* ions could be improved by changing the lattice parameters of host [27]. The ionic radius of Sr^{2+} is larger than that of Ln^{3+}, and thus, some superior features can be expected in $NaYF_4$:Ln^{3+} nanocrystals by codoping with Sr^{2+} ions. In this study, $NaYF_4$:Eu/Sr nanocrystals have been synthesized, using a solution–liquid–solid (LSS) technique. Eu^{3+} and Eu^{2+} have been found to coexist in the Eu/Sr-codoped $NaYF_4$ nanocrystals. The Eu^{3+}/Eu^{2+} emission intensity ratio changed with the Sr^{2+} concentration as well as the excitation wavelength. Spectral analysis indicates that the material has multiple luminescence centers or emitting states.

2. Experiments

In a typical synthesis, 1.5 mL of an NaF aqueous solution (0.5 mol/L) and 0.5 mL of nitrate [$Y(NO_3)_3$, $Eu(NO_3)_3$, and $Sr(NO_3)_2$] aqueous solution (0.5 mol/L) were added to a mixture of NaOH (1.2 g), ethanol (10 mL), deionized water (8 mL), and oleic acid (20 mL), and the solution was thoroughly stirred. Subsequently, the milky colloidal solution was transferred to a 50 mL Teflon-lined autoclave, and heated at 160 °C for 14 h. The systems were then allowed to cool to room temperature. The final products were collected by means of centrifugation, washed with ethanol, and finally dried in vacuum at 80 °C for 4 h.

Characterization: the crystal structure was analyzed by a Rigaku RU-200b X-ray powder diffractometer (XRD), using a nickel-filtered Cu $K\alpha$ radiation ($\lambda = 1.5418$ Å). The size and morphology of the final products were characterized with a Hitachi H-800 transmission electron microscope (TEM), operated at 200 kV. Samples were prepared by placing a drop of dilute cyclohexane dispersion of the nanocrystals on the surface of a copper grid. The luminescence spectra were recorded with a Hitachi F-4500 fluorescence spectrophotometer at room temperature. For comparison of the luminescence properties of different samples, the luminescence spectra were measured with the same instrument parameters (5 nm for slit width and 400 V for PMT voltage).

3. Results and discussion

3.1. Crystal structure and morphology

Fig. 1 shows the XRD patterns of the as-prepared $NaYF_4$:Sr/Eu nanocrystals with different Sr^{2+} concentration. It is noted that the

* Corresponding author. Fax: +86 10 62792798.
E-mail address: pengqing@tsinghua.edu.cn (Q. Peng).

0022-4596/$ - see front matter © 2010 Elsevier Inc. All rights reserved.
doi:10.1016/j.jssc.2010.10.030

concentration refers to the initial Sr^{2+} concentration of reactant. The diffraction peaks in curve 1*a* can be indexed to pure cubic phase $NaYF_4$ (JCPDS 06-0342). The very weak diffraction peaks marked by asterisks arise from the hexagonal phase $NaYF_4$ (JCPDS 16-0334). The positions of all diffraction peaks of the nanocrystals can be observed to shift toward larger lattice parameters with increasing Sr^{2+} concentration, indicating the lattice expansion as a result of Sr^{2+} incorporation. Although the valences of Y^{3+} and Sr^{2+} are different, they can be replaced each other with the help of charge compensation. This result is similar to the SrF_2–YF_3 or CaF_2–YF_3 systems reported by Achary et al. [28]. In addition, from bottom to top in Fig. 1, the XRD patterns become broader and broader, suggesting that the crystalline size gradually decreases with increasing Sr^{2+} concentration. Both $NaYF_4$ and SrF_2 are cubic phases, and thus, similar crystal structures can be observed in samples with different concentration.

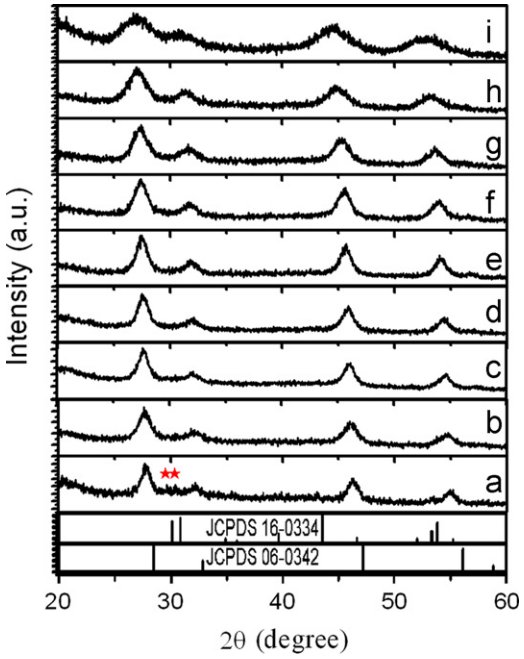

Fig. 1. XRD patterns of $NaYF_4$:Sr/Eu nanocrystals with different Sr^{2+} concentration (10% Eu): (a) 0%, (b) 1%, (c) 5%, (d) 15%, (e) 30%, (f) 40%, (g) 50%, (h) 70%, and (i) 80%.

The morphologies of the final products were characterized with a Hitachi H-800 transmission electron microscope (TEM) operated at 200 kV. Fig. 2a shows the TEM image of $NaYF_4$:Sr(30%)/Eu(10%) nanocrystals. They are monodisperse, with a diameter of ~10 nm. The high-resolution transmission electron microscope (HRTEM) image of a single nanoparticle is shown in Fig. 2b. The measured lattice spacing is about 0.323 nm, which reveals the single-crystal nature of the product. Fig. 2c shows the TEM image of $NaYF_4$:Sr(70%)/Eu(10%) nanocrystals. The mean diameter of nanoparticles is ~5nm. Obviously, the particle size of an $NaYF_4$:Sr(70%)/Eu(10%) is less than that of $NaYF_4$:Sr(30%)/Eu(10%) nanocrystals, which is in accordance with the XRD analysis. During the HRTEM measurement, the elemental components of the nanocrystals were detected by an energy-dispersive X-ray analysis (EDXA). The EDXA result confirmed that the elemental components are Sr, Y, Eu, Na, and F (Fig. 2d). The actual Sr^{2+} concentration is almost consistent with the initial dopant concentration of the reactant.

3.2. Luminescence characteristics

3.2.1. Tunable luminescence of Eu^{2+}/Eu^{3+} in $NaYF_4$ nanocrystals by Sr^{2+} codoping

Fig. 3 shows the emission spectra of $NaYF_4$:Sr/Eu nanocrystals under 396 nm excitation, which corresponds to the $^7F_0 \rightarrow {}^5L_6$ transition of Eu^{3+}. The emissions of Eu^{3+} and Eu^{2+} were observed simultaneously. The results demonstrate the coexistence of Eu^{2+} and Eu^{3+} ions in the samples. The emission peaks located in the

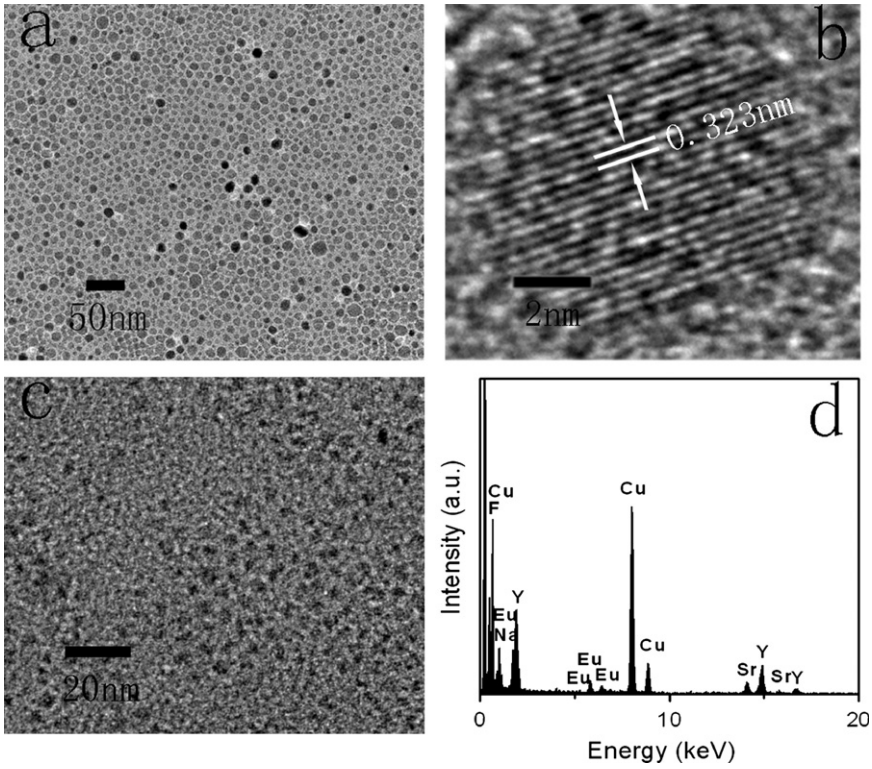

Fig. 2. (a) TEM and (b) HRTEM images of $NaYF_4$:Sr(30%)/Eu(10%) nanocrystals. (c) TEM image of $NaYF_4$:Sr(70%)/Eu(10%) nanocrystals. (d) An EDXA pattern of $NaYF_4$:Sr(30%)/Eu(10%) nanocrystals.

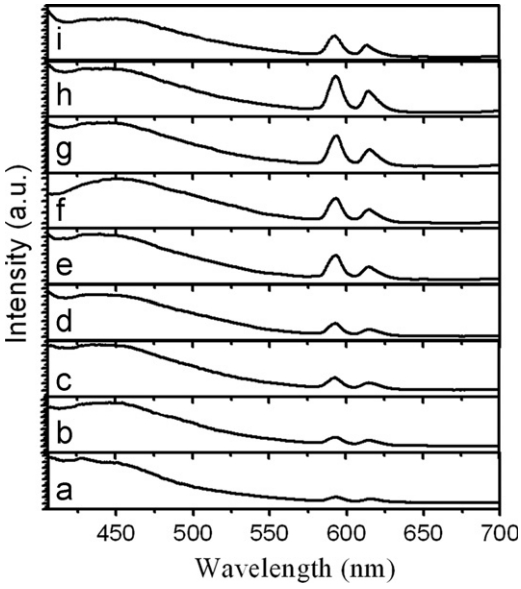

Fig. 3. Emission spectra (λ_{ex}=396 nm) of $NaYF_4$:Sr/Eu nanocrystals with different Sr^{2+} concentration (10% Eu): (a) 0%, (b) 1%, (c) 5%, (d) 15%, (e) 30%, (f) 40%, (g) 50%, (h) 70%, and (i) 80%.

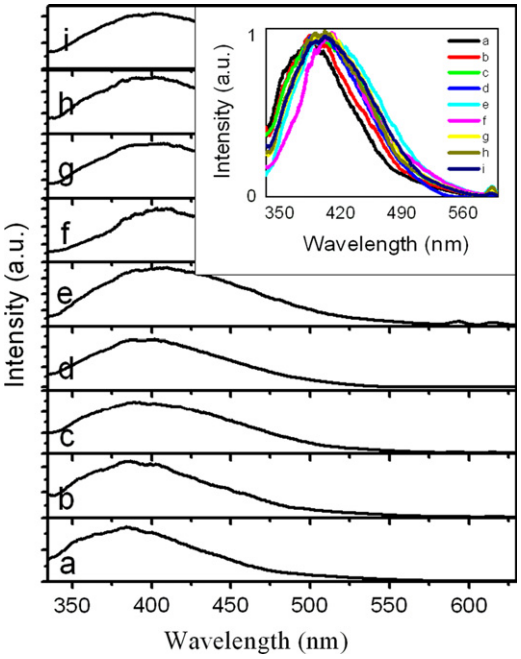

Fig. 4. Emission spectra (λ_{ex}=325 nm) of $NaYF_4$:Sr/Eu nanocrystals with different Sr^{2+} concentration (10% Eu): (a) 0%, (b) 1%, (c) 5%, (d) 15%, (e) 30%, (f) 40%, (g) 50%, (h) 70%, and (i) 80%. An inset shows the normalized emission spectra in the range 334–600 nm.

575–630 nm range can be attributed to the $^5D_0 \rightarrow {}^7F_1$ and $^5D_0 \rightarrow {}^7F_2$, which are typical magnetic and electric dipole–dipole transitions of Eu^{3+}, respectively. In a site with an inversion symmetry the $^5D_0 \rightarrow {}^7F_1$ is dominating, while in a site without an inversion symmetry, the $^5D_0 \rightarrow {}^7F_2$ is the strongest. Therefore, the intensity ratio of $^5D_0 \rightarrow {}^7F_2$–$^5D_0 \rightarrow {}^7F_1$ is strongly dependent on the local symmetry of the Eu^{3+} ions. By comparing the emission intensity of the $^5D_0 \rightarrow {}^7F_1$ with that of the $^5D_0 \rightarrow {}^7F_2$ in Fig. 3, it is inferred that the Eu^{3+} ions in $NaYF_4$:Sr/Eu nanocrystals occupy a site with a small deviation from an inversion symmetry. The peak positions of Eu^{3+} were independent of Sr^{2+} concentration.

In addition to the aforementioned emissions of Eu^{3+}, a very strong emission band centered at ~450 nm was also observed, which corresponds to the transition from the $4f^65d$ to $4f^7$ configuration of Eu^{2+} [29,30]. The Eu^{2+} emission in different hosts lies in characteristically different ranges due to different structures. The Eu^{3+}/Eu^{2+} emission intensity ratio increases with increasing Sr^{2+} concentration, up to about 70 mol%, and then decreases.

Fig. 4 shows the emission spectra of $NaYF_4$:Sr/Eu nanocrystals under 325 nm excitation, which corresponds to the 5d–4f emission of Eu^{2+}. The inset of Fig. 4 is the magnification of the spectra in the range 334–600 nm. It is observed that the emission of Eu^{2+} is much stronger than that of Eu^{3+}. With the increase of Sr^{2+} concentration, this broadband emission of Eu^{2+} experiences a slight bathochromic shift first, then the inverse tendency.

Fig. 5 shows the excitation (monitored at 592 nm) spectra of $NaYF_4$:Sr/Eu nanocrystals, which consist of the characteristic excitation lines of Eu^{3+}. These excitation lines can be clearly assigned: $^7F_0 \rightarrow {}^5H_6$ (~320 nm), $^7F_0 \rightarrow {}^5D_4$ (~364 nm), $^7F_0 \rightarrow {}^5G_2$ (~382 nm), $^7F_0 \rightarrow {}^5L_6$ (~396 nm), $^7F_0 \rightarrow {}^5D_2$ (~467 nm), $^7F_0 \rightarrow {}^5D_1$ (~537 nm), and $^7F_0 \rightarrow {}^5D_0$ (~565 nm). Fig. 6 shows the excitation (monitored at 452 nm) spectra of $NaYF_4$:Sr/Eu nanocrystals with different Sr^{2+} concentration, which consist of the characteristic excitation bands of Eu^{2+}. As mentioned above, the Eu^{2+} emission in different hosts lies in characteristically different ranges due to different structures. These spectral configurations of Eu^{2+} are different, indicating that the local symmetry of the Eu^{2+} ions is changed by codoping with Sr^{2+} ions. It is imperative to point out that the excitation peaks corresponding to the $^7F_0 \rightarrow {}^5F_2$ and $^7F_0 \rightarrow {}^5H_6$ of an Eu^{3+} overlapped with the transitions of Eu^{2+}. In addition, the excitation spectra monitored at 426 and 452 nm have similar behaviors.

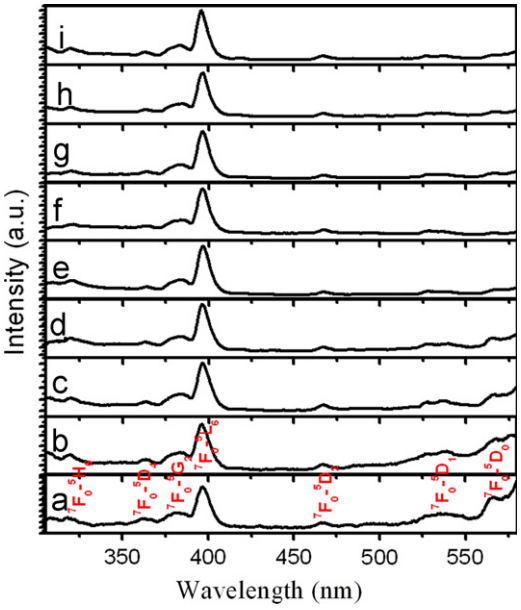

Fig. 5. Excitation spectra (λ_{em}=592 nm) of $NaYF_4$:Sr/Eu nanocrystals with different Sr^{2+} concentration (10% Eu): (a) 0%, (b) 1%, (c) 5%, (d) 15%, (e) 30%, (f) 40%, (g) 50%, (h) 70%, and (i) 80%.

3.2.2. *Tunable luminescence of $NaYF_4$:Sr(70%)/Eu(10%) nanocrystals by exciting at different wavelengths*

Fig. 7a shows the emission spectra of $NaYF_4$:Sr(70%)/Eu(10%) nanocrystals, when the Eu^{3+} ions were excited. Fig. 7b shows the emission spectra of $NaYF_4$:Sr(70%)/Eu(10%) nanocrystals, when the Eu^{2+} ions were excited. It is clearly observed that all the spectra consist of the emissions of Eu^{3+} and Eu^{2+}. We suggested that this

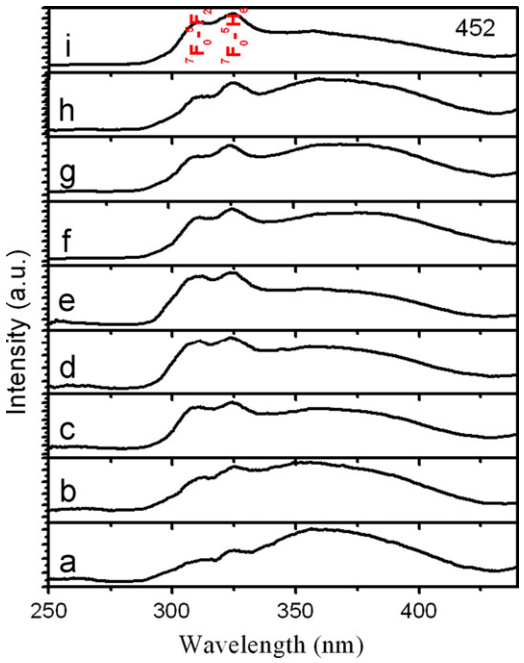

Fig. 6. Excitation spectra (λ_{em}=452 nm) of $NaYF_4$:Sr/Eu nanocrystals with different Sr^{2+} concentration (10% Eu): (a) 0%, (b) 1%, (c) 5%, (d) 15%, (e) 30%, (f) 40%, (g) 50%, (h) 70%, and (i) 80%.

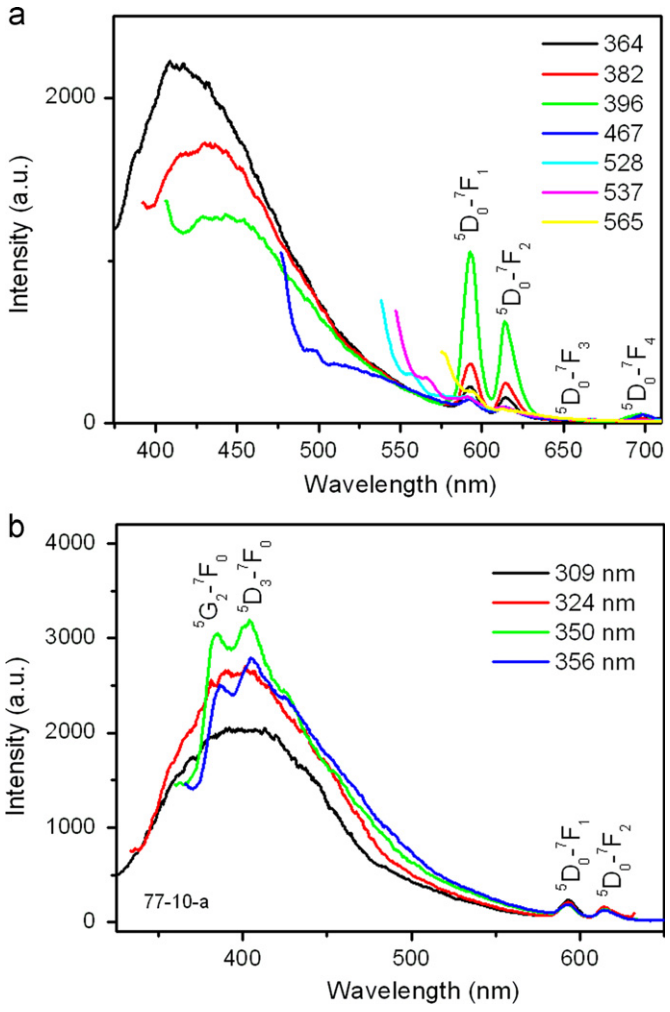

Fig. 7. Emission spectra of $NaYF_4$:Sr(70%)/Eu(10%) nanocrystals under different excitation wavelength.

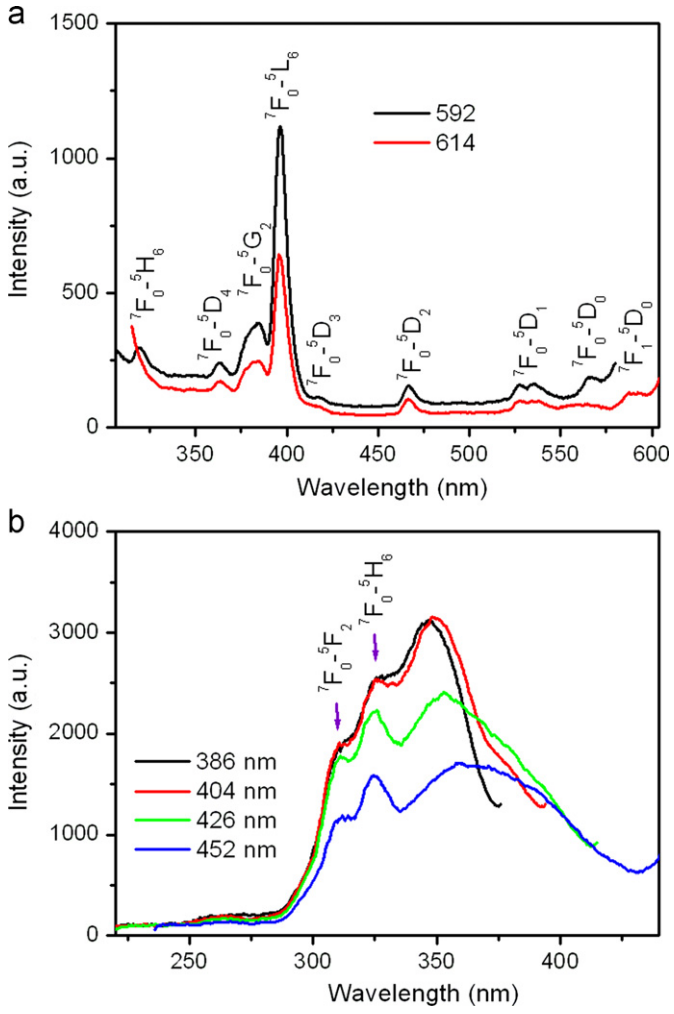

Fig. 8. Excitation spectra of $NaYF_4$:Sr(70%)/Eu(10%) nanocrystals monitored at different emission wavelength.

phenomenon can be attributed to the spectral overlapping and energy transfer between Eu^{3+} and Eu^{2+} ions. The Eu^{3+}/Eu^{2+} emission intensity ratio changes with an excitation wavelength. When the Eu^{2+} ions were excited (λ_{ex}=309, 324, 350, and 356 nm), the emissions from Eu^{3+} are very weak. When the Eu^{3+} ions were excited (λ_{ex}=364, 396, 467, 528, 537, and 565 nm), the emissions from Eu^{3+} become stronger. The emission intensities of Eu^{3+} ions were the strongest when the excitation was performed at 396 nm. In addition, the spectral configurations of Eu^{2+} are also changing with excitation wavelength. This is a normal phenomenon when the material has multiple luminescence centers or emitting states.

Fig. 8 shows the excitation spectra of $NaYF_4$:Sr(70%)/Eu(10%) nanocrystals monitored at different excitation wavelengths. For Eu^{3+} ions (Fig. 8a), the strongest excitation peak of Eu^{3+} is found to be located at 396 nm ($^7F_0 \rightarrow {}^5L_6$), which is in accordance with the excitation spectrum of cubic $NaYF_4$:Eu^{3+} nanocrystals reported previously. For Eu^{2+} ions (Fig. 8b), it was observed that two shoulders appeared in the short wavelength side of the excitation band of Eu^{2+}, which correspond to the $^7F_0 \rightarrow {}^5F_2$ and $^7F_0 \rightarrow {}^5H_6$ transitions. The emission band of an Eu^{2+} shifted towards longer wavelength, when a longer wavelength emission was monitored. The positions of the shoulders were independent of excitation wavelength. These spectral phenomena have been observed for all the samples.

4. Conclusion

Eu/Sr-codoped $NaYF_4$ nanocrystals have been synthesized by an LSS process. The positions of XRD peaks of the nanocrystals shifted towards larger lattice parameters with increasing Sr^{2+} concentration. Furthermore, the particle size decreased with increasing Sr^{2+} concentration. The influence of Sr^{2+} concentration on the luminescence of $NaYF_4$:Eu/Sr nanocrystals was studied systemically. The emissions of Eu^{3+} and Eu^{2+} were observed simultaneously, revealing that Eu^{3+} and Eu^{2+} coexist in Eu/Sr-codoped $NaYF_4$ nanocrystals. The Eu^{3+}/Eu^{2+} emission intensity ratio not only changed with the Sr^{2+} concentration, but also changed with the excitation wavelength. The spectral configurations of Eu^{2+} and Eu^{3+} also varied with the excitation wavelength, indicating that the material has multiple luminescence centers or emitting states.

Acknowledgments

This work was supported by the State Key Project of Fundamental Research for Nanoscience and Nanotechnology (2011CB932401), the Foundation for Innovative Research Groups of the National Natural Science Foundation of China (20921001), and the National Natural Science Foundation of China (10979032).

References

[1] R. Yan, Y. Li, Adv. Funct. Mater. 15 (2005) 763–770.
[2] G. De, W. Qin, J. Zhang, J. Zhang, Y. Wang, C. Cao, Y. Cui, J. Lumin. 122 (2007) 128–130.
[3] G. Wang, W. Qin, J. Zhang, J. Zhang, Y. Wang, C. Cao, L. Wang, G. Wei, P. Zhu, R. Kim, J. Phys. Chem. C 112 (2008) 12161–12167.
[4] G. Wang, W. Qin, Y. Xu, L. Wang, G. Wei, P. Zhu, R. Kim., J. Fluorine Chem. 129 (2008) 1110–1113.
[5] Z. Hou, P. Yang, C. Li, L. Wang, H. Lian, Z. Quan, J. Lin, Chem. Mater. 20 (2008) 6686–6696.
[6] J. Yang, C. Li, Z. Cheng, X. Zhang, Z. Quan, C. Zhang, J. Lin, J. Phys. Chem. C 111 (2007) 18148–18154.
[7] C. Li, J. Yang, P. Yang, H. Lian, J. Lin, Chem. Mater. 20 (2008) 4317–4326.
[8] C. Li, J. Yang, Z. Quan, P. Yang, D. Kong, J. Lin, Chem. Mater. 19 (2007) 4933–4942.
[9] C. Li, Z. Quan, P. Yang, J. Yang, H. Lian, J. Lin, J. Mater. Chem. 18 (2008) 1353–1361.
[10] G. De, W. Qin, J. Zhang, D. Zhao, J. Zhang, Chem. Lett. 34 (2005) 1–3.
[11] Y. Wang, W. Qin, J. Zhang, C. Cao, J. Zhang, Y. Jin, P. Zhu, G. Wei, G. Wang, L. Wang, Chem. Lett. 36 (2007) 1–3.
[12] M. Wang, Q. Huang, H. Zhong, X. Chen, Z. Xue, X. You, Cryst. Growth Des. 7 (2007) 2106–2111.
[13] Y. Sun, Y. Chen, L. Tian, Y. Yu, X. Kong, J. Zhao, H. Zhang, Nanotechnology 18 (2007) 275609/1-9.
[14] F. Tao, Z. Wang, L. Yao, W. Cai, X. Li, Growth Des. 7 (2007) 854–858.
[15] X. Bai, H. Song, G. Pan, Y. Lei, T. Wang, X. Ren, S. Lu, B. Dong, Q. Dai, L. Fan, J. Phys. Chem. C 111 (2007) 13611–13617.
[16] Y. Kim, Y. Yang, S. Ha, S. Cho, Y. Kim, H. Kim, H. Yang, Y. Kim, Sensors Actuators B 106 (2005) 189–198.
[17] R. Bhargava, D. Gallaghar, X. Hong, A. Nurmikko, Phys. Rev. Lett. 72 (1994) 416–419.
[18] J. Zhuang, L. Liang, H. Sung, Z. Yang, M. Wu, L. Williams, S. Feng, Q. Su, Inorg. Chem. 46 (2007) 5404–5410.
[19] L. Wang, Y. Li, Chem. Mater. 19 (2007) 727–734.
[20] L. Wang, Y. Li, Nano Lett. 6 (2006) 1645–1649.
[21] L. Gao, X. Ge, Z. Chai, G. Xu, X. Wang, C. Wang, Nano Res. 2 (2009) 565–574.
[22] X. Sun, Y. Li, Chem. Commun. 34 (2003) 1768–1769.
[23] G. Wang, Q. Peng, Y. Li, J. Am. Chem. Soc. 131 (2009) 14200–14201.
[24] P. Li, Q. Peng, Y. Li, Adv. Mater. 21 (2009) 1945–1948.
[25] C. Cao, W. Qin, J. Zhang, Y. Wang, P. Zhu, G. Wang, G. Wei, L. Wang, L. Jin, J. Fluorine Chem. 129 (2008) 204–209.
[26] Y. Liu, A. Tu, H. Zhu, R. Li, W. Luo, X. Chen, Adv. Mater. 10.1002/adma.201000128.
[27] G. Wang, W. Qin, D. Zhang, L. Wang, G. Wei, P. Zhu, R. Kim, J. Phys. Chem. C 112 (2008) 17042–17045.
[28] S. Achary, S. Patwe, A. Tyagi, Mater. Res. Bull. 37 (2002) 2227–2241.
[29] Y. Su, L. Li, G. Li, Cryst. Growth Des. 8 (2008) 2678–2683.
[30] Y. Huang, H. You, G. Jia, Y. Zheng, Y. Song, M. Yang, K. Liu, L. Zhang, J. Phys. Chem. C 113 (2009) 16962–16968.